Heliyon 9 (2023) e22505

Contents lists available at ScienceDirect

Heliyon

journal homepage: www.cell.com/heliyon

Numerical study for bioconvection peristaltic flow of Sisko nanofluid with Joule heating and thermal radiation

Zahid Nisar [a,*], Bilal Ahmed [b], Hassan Ali Ghazwani [c,**], Khursheed Muhammad [d], Mohamed Hussien [e], Arsalan Aziz [f]

[a] *Department of Computer Science, National University of Sciences and Technology (NUST), Balochistan Campus (NBC), Quetta, 87300, Pakistan*
[b] *School of Energy and Power Engineering, Jiangsu University, Zhenjiang, 212013, China*
[c] *Department of Mechanical Engineering, Faculty of Engineering, Jazan University, P.O. Box 45124, Jazan, Saudi Arabia*
[d] *Department of Humanities and Sciences, School of Electrical Engineering and Computer Science (SEECS), National University of Sciences and Technology (NUST), Islamabad, Pakistan*
[e] *Department of Chemistry, Faculty of Science, King Khalid University, P.O. Box 9004, Abha, 61413, Saudi Arabia*
[f] *Department of Mathematics, Quaid-I-Azam University, Islamabad, Pakistan*

ARTICLE INFO

Keywords:
Numerical solutions
Peristalsis
Bioconvection
Sisko fluid model
Nanofluid
Thermal radiation

ABSTRACT

Present work describes the peristaltic flow of Sisko nanomaterial with bioconvection and gyrotactic microorganisms. Slip conditions are incorporated through elastic channel walls. Additionally, we considered the aspects of thermal radiation and viscous dissipation. Further ohmic heating features are also present in the thermal field. Buongiorno's nanofluid model comprising thermophoresis and Brownian movement is taken. The lubrication approach is utilized for the simplification of the problem. Being highly coupled and nonlinear, the resulting system of equations must be solved numerically using the NDSolve technique and bvp4c via Matlab. Velocity, concentration, thermal field and motile microorganisms. are addressed graphically.

1. Introduction

Nanofluids are a suspension of nanometer-sized metallic particles (<100 nm) in a base fluid, such as water. Poor thermal conductivity is the main problem that occurs in the process of heat transfer in many advanced industries and technologies. Therefore the researchers use the composition of nanoparticles with base fluid to enhance the thermophysical characteristics of the base liquid to overcome the heat transfer issues. Nanoliquids' excellent thermophysical properties, such as thermal conductivity and diffusivity, are essential to a wide screen of commercial processes, permitting transportation, thermosyphons, reactors of nuclear, biotechnology and heat pulsing pipes. Additionally, it is used in chemotherapy to eradicate viral censorial cells. Some environmentally friendly technologies, such as the small quantity of oil and leaser quantity of cooling grease make use of nanofluids to lessen the demand for drilling fluids while enhancing common cooling and lubricating properties. Initially, the term "nanofluid" was created by Choi and Eastman [1] to refer to the usage of nano-sized diameter less than 100 nm part diameters conventional fluids. In Buongiorno's [2] comprehensive investigation of nanofluids, he examines the mechanisms behind the enhancement of thermal conductivity resulting from the Brownian motion and thermophoretic scattering of nanoparticles. Ijam and Saidur [3] explored how nanoparticles are used as a

* Corresponding author.
** Corresponding author.
E-mail addresses: nisarzahid@yahoo.com (Z. Nisar), hghazwani@jazanu.edu.sa (H.A. Ghazwani).

https://doi.org/10.1016/j.heliyon.2023.e22505
Received 26 June 2023; Received in revised form 13 November 2023; Accepted 14 November 2023
Available online 22 November 2023

coolant in electronic devices. Mustafa et al. [4] examined the peristaltic flow of nanoliquid with the features of induced magnetic effects. Hayat et al. [5] discussed the peristaltic motion of nanoliquid with convective and wall properties. Ohmic heating and flexible wall characteristics in MHD peristaltic flow were scrutinized by Sucharitha et al. [6]. Abbasi et al. [7] discovered how effective thermal properties are pertinent to nanoparticles (Au, Ag, Fe3O4) in peristalsis. Akram et al. [8] studied the MHD peristaltic activity of Prandtl nanofluids considering the aspects of mass and thermal convection. Hayat et al. [9] described the aspects of mixed convection for peristaltic motion of Sutterby nanoliquid. Khazayinejad et al. [10] looked at graphene-blood nanoliquid in peristaltic activity by taking thermal radiation through porous space. Kotnurkar and Talawar [11] reported the MHD peristaltic activity of Jeffrey nanoliquid in a eccentric annulus. Further, a few updated and relevant studies in this direction can be cited through [12–17].

Peristalsis is an instantaneous muscle contraction and relaxation process that occurs in waves, for instance, in the esophagus where food boluses are swallowed and moved through various digestive tract processing units. In peristaltic pumps, where various kinds of fluids are displaced, peristalsis also takes place. The subject of peristalsis has captured the attention of latest research due to its well-known implementation in the sectors of burning, industrial equipment, engineering of chemical, biomaterials, and physiology. The liquid is pumped through a process termed peristalsis, which is built on sine wave transmission. Peristaltic transport of nano fluid is essential in biological and technical processes. The peristaltic movement is used in many physiological processes, including embryo transport, bile ducts motion, blood stream through capillaries, and many more. Theoretical and experimental research methods were employed by Latham [18] in his initial survey of peristaltic motion, keeping the resulting implications in focus. Following this, a multitude of researchers have explored a range of peristalsis-related subjects in different flow scenarios. Shapiro et al. [19] broadened the investigation of peristaltic pumping by utilizing the “small Reynolds numberand large wavelength assumption”. Srinivas and Kothandapani [20] discussed the transfer of heat analysis of peristalsis activity in a canal. Ali et al. [21] scrutinized the numerical investigation of peristaltic motion of curved channel. Peristaltic motion of mass and heat transfer with considering the features of induced magnetic aspects followed by Hayat et al. [22]. Abbasi et al. [23] investigated the numerical inquiry for MHD peristaltic movement Carreau-Yasuda material in a curvical tube with aspects of Hall current. Sinnott et al. [24] analyzed the peristaltic activity of a particulate interruption in the trifling intestine. Rashid et al. [25] examined the MHD peristaltic flow of Williamson material cindering curved channel. Akbar and Abbasi [26] explored the aspects of entropy generation in peristaltic transport. Slip and Hall investigated the peristaltic movement of Jeffrey liquid through porous space were analyzed by Gangavathi et al. [27]. Nisar et al. [28] studied the chemically reactive peristaltic transportation of couple stress nanomaterial. In the study of the peristaltic process, the effects of wall features such as surface stiffness, viscous damping force, wall stiffness have become increasingly important. Some relevant investigation regarding this study is listed through [29–31].

Scientists and engineers have started to pay more attention to the study of non-Newtonian liquid models in past years because it addresses many fundamental issues from the biomedical sciences, geoscience, petrochemical, and petroleum industries, among other fields. In contrast to the Navier-Stokes equations, in non-Newtonian materials, the intrinsic interactions amongst stress and rate of stress are more intricate. Due to the complexity of non-Newtonian liquids, it is impossible to anticipate all of their diverse properties. It is possible to utilize non-Newtonian liquid models to illustrate the typical flow behavior of liquids found in both industry and society. As an outcome, various engineers and academics described various fluid systems. Out of these options, the Sisko fluid model [32] can elucidate the characteristics of shear thinning and thickening. Akbar [33] investigated how Sisko fluid moved peristaltically inside an asymmetric tube. Bhatti et al. [34] scrutinized the endoscopic features of peristaltic Sisko blood flow of titanium magneto-nanoparticles. Mathematical modeling of peristaltic transport of Sisko material considering porous space was studied by Asghar e al [35]. The mixed convection flows peristaltic flow of Sisko nano liquid with heat flow was studied by Ahmed et al. [36]. Sisko fluid’s peristaltic movement with double-diffusive convection was covered by Akram et al. in their study [37]. Numerical examine of Sisko mterial for hybrid nanomaterials is analyzed by Almaneea [38]. Tanveer and Ashraf [39] reported the entropy generation of Sisko fluid with Joule heating.

The formation of suspensions generation of microorganisms, such as bacteria and algae, is what is meant by the term “bio-convection.” The movement of microorganisms results in bioconvection. Microorganisms that are typically 5–10 % denser than water move upward in a process known as bioconvection. The primary fluid density is raised by the presence of these self-moving motile bacteria. Bioconvection is employed in a broad range of applications, including organic implementations and microsystems, the pharmaceutical industry, biopolymer manufacturing, applications that are safe for the environment. Also advances in the use of economical energy sources, oil recovery of oil in progressed microbial, biotechnology, biosensors and continuous numeral presenting. Few pertinent studies is cited in Refs. [40–45].

We investigate the magnetohydrodynamics (MHD) [46–50] bioconvection peristaltic activity of Sisko nanofluid by considering gyrotactic microorganisms. Partial slip characteristics are imposed on elastic channel. Aspects of Joule heating and thermal radiation are also present in thermal field equation. Numerical solutions are accomplished by using NDSolve from Mathematica and bvp4c by using MATLAB. The effects of distinct involved variables are scrutinized by plotting the graphs of temperature, velocity, concentration and gyrotactic microorganisms profile. Finally, a comparison of heat transfer rate is evaluated via numerical investigation.

2. Formulation

We examine the peristaltic activity of Sisko nanoliquid having channel width $2d_1$. We pick out Cartesian coordinates in this a manner that sinusoidal waves travel in $x-$ direction which is parallel to the walls of the channel and $y-$ axis is taken vertical to it. By introducing a magnetic field (of constant strength and constant B_0) in the y-direction, fluid becomes electrically conductive. As a result of the low magnetic Reynolds amount, electric field impacts are supposed to be zero. Sinusoidal waves that are moving along the elastic walls of the channel at a constant rate c serve as the source of the flow inside it. The wall shapes are [5]

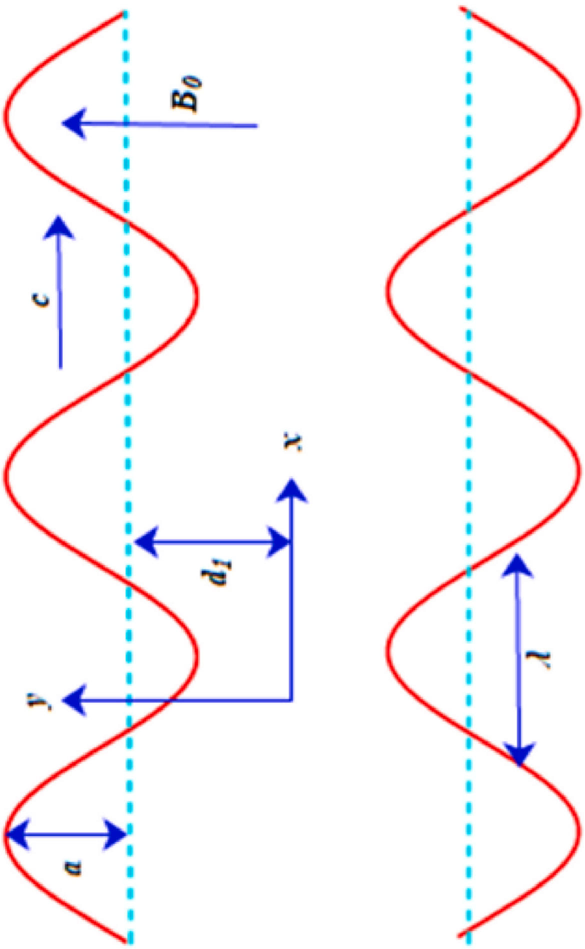

Fig. 1. Geometry of the problem.

$$y = \pm\eta(x,t) = \pm\left[d_1 + a\sin\frac{2\pi}{\lambda}(x - ct)\right], \tag{1}$$

where a and λ represents amplitude and length of wave respectively. (See Fig. 1).

The pertained formulations for Sisko liquid **S** outlined by [36]

$$\mathbf{S} = \left[\alpha + \varsigma\sqrt{\dot{\gamma}}^{\,n-1}\right]\mathbf{A}_1, \tag{2}$$

$$\dot{\gamma} = \frac{1}{2}tr\mathbf{A}_1^2, \tag{3}$$

$$\mathbf{A}_1 = (\mathrm{grad}V) + (\mathrm{grad}V)^t, \tag{4}$$

where α and ς denote material constants and $\mathbf{A}_1$ the first Rivlin Ericksen tensor. In addition, the channel boundaries are being taken into account with elastic properties. The continuity, momentum, energy, concentration and microorganism eqautions are listed below [5,17,26,36]

$$\frac{\partial u}{\partial x} + \frac{\partial v}{\partial y} = 0, \tag{5}$$

$$\begin{aligned}\rho_f\left(\frac{\partial u}{\partial t} + u\frac{\partial u}{\partial x} + v\frac{\partial u}{\partial y}\right) &= -\frac{\partial p}{\partial x} + \frac{\partial S_{xx}}{\partial x} + \frac{\partial S_{xy}}{\partial y} - \sigma B_0^2 u \\ &+ g(1 - F_0)\rho_f\beta_T(T - T_0) - (\rho_p - \rho_f)g\beta_c(C - C_0) - (\rho_m - \rho_f)\gamma g(F - F_0),\end{aligned} \tag{6}$$

$$\rho_f\left(\frac{\partial v}{\partial t}+u\frac{\partial v}{\partial x}+v\frac{\partial v}{\partial y}\right)=-\frac{\partial p}{\partial y}+\frac{\partial S_{yx}}{\partial x}+\frac{\partial S_{yy}}{\partial y}-\sigma B_0^2 v, \tag{7}$$

$$\begin{aligned}\left(\frac{\partial T}{\partial t}+u\frac{\partial T}{\partial x}+v\frac{\partial T}{\partial y}\right)=\alpha\left(\frac{\partial^2 T}{\partial x^2}+\frac{\partial^2 T}{\partial y^2}\right)+\frac{1}{\rho_f c_f}\left\{\frac{\partial u}{\partial x}S_{xx}+\left(\frac{\partial u}{\partial y}+\frac{\partial v}{\partial x}\right)S_{xy}+\frac{\partial v}{\partial y}S_{yy}\right\}\\ +\tau\left[D_B\left(\frac{\partial C}{\partial y}\frac{\partial T}{\partial y}+\frac{\partial C}{\partial x}\frac{\partial T}{\partial x}\right)+\frac{D_T}{T_m}\left\{\left(\frac{\partial T}{\partial y}\right)^2+\left(\frac{\partial T}{\partial x}\right)^2\right\}\right]-\frac{\partial q_r}{\partial y}+\frac{1}{\rho_f c_f}\sigma B_o^2 u^2,\end{aligned} \tag{8}$$

$$\frac{\partial C}{\partial t}+u\frac{\partial C}{\partial x}+v\frac{\partial C}{\partial y}=D_B\left(\frac{\partial^2 C}{\partial x^2}+\frac{\partial^2 C}{\partial y^2}\right)+\frac{D_T}{T_m}\left(\frac{\partial^2 T}{\partial x^2}+\frac{\partial^2 T}{\partial y^2}\right). \tag{9}$$

$$\frac{\partial F}{\partial t}+u\frac{\partial F}{\partial x}+v\frac{\partial F}{\partial y}=D_N\left(\frac{\partial^2 F}{\partial x^2}+\frac{\partial^2 F}{\partial y^2}\right)-\left(\frac{\partial}{\partial x}\left(F\frac{\partial C}{\partial x}\right)\frac{bW_c}{(C_1-C_0)}+\frac{\partial}{\partial y}\left(F\frac{\partial C}{\partial y}\right)\right). \tag{10}$$

The subjected boundary conditions are

$$u\pm\beta_1 S_{xy}=0 \text{ at } y=\pm\eta, \tag{11}$$

$$\begin{aligned}\left(-\tau_1\frac{\partial^3}{\partial x^3}+m_1\frac{\partial^3}{\partial x\partial t^2}+d\frac{\partial^2}{\partial t\partial x}\right)\eta=\frac{\partial S_{xx}}{\partial x}+\frac{\partial S_{xy}}{\partial y}-\rho_f\left(\frac{\partial u}{\partial t}+u\frac{\partial u}{\partial x}+v\frac{\partial u}{\partial y}\right)-\\ \sigma B_0^2 u+g(1-F_0)\rho_f\beta_T(T-T_0)-(\rho_p-\rho_f)g\beta_C(C-C_0)-(\rho_m-\rho_f)g\gamma(F-F_0) \text{ at } y=\pm\eta,\end{aligned} \tag{12}$$

$$T\pm\beta_2\frac{\partial T}{\partial y}=\begin{Bmatrix}T_1\\T_0\end{Bmatrix}, C\pm\beta_3\frac{\partial C}{\partial y}=\begin{Bmatrix}C_1\\C_0\end{Bmatrix}, F=\begin{Bmatrix}F_1\\F_0\end{Bmatrix} \text{at} y=\pm\eta. \tag{13}$$

Here (v,u) are velocity components in (y,x) plane, (ρ_p) the nanoparticles density, (D_N) the microorganisms diffusion coefficient, (ρ_f) the density of nanofluid, (ρ_m) the motile microorganisms density, (g) the gravity, (ν) for kinematic viscosity, (σ) for electric conductions, (α) the thermal diffusivity, (p) for pressure. Further (D_B) Brownian motion coefficient and (D_T) describes for thermophoretic diffusion, (W_c) the maximum cell swimming speed, (τ_1) for tension of ealstic, (b) the chemotaxis constant, (m_1) for area per unit mass, (T_m) for mean temperature, (γ) the average volume of microorganisms, (d) for viscous damping coefficient, (T_1,T_0) and (C_1,C_0) are temperature concentration at the upper and lower walls respectively. Moreover, (F_1,F_0) the volume fraction at upper and lower walls. The q_r is defined by [28]

$$q_r=-\frac{4\bar{\sigma}}{3\bar{k}}\frac{\partial T^4}{\partial y}, \tag{14}$$

where $\bar{\sigma}$ and $\bar{k}$ are the coefficients of Stefan-Boltzman and absorption of mean. Expand form of T^4 can be defined as

$$T^4=4T_0^3T-3T_0^4, \tag{15}$$

thus we have

$$q_r=-\frac{16\bar{\sigma}T_0^3}{3\bar{k}}\frac{\partial T}{\partial y}. \tag{16}$$

Considering stream function $u=\psi_y,\ v=-\delta(\psi_x)$ and using the non-dimensional variables [45]

$$\begin{aligned}&u^*=\frac{u}{c}, v^*=\frac{v}{c}, x^*=\frac{x}{\lambda}, y^*=\frac{y}{d_1}, t^*=\frac{ct}{\lambda}, \eta^*=\frac{\eta}{d_1},\\ &p^*=\frac{d_1^2 p}{c\lambda\mu}, \theta=\frac{T-T_0}{T_1-T_0}, \phi=\frac{C-C_0}{C_1-C_0}, \beta_1^*=\frac{\beta_1\alpha}{d_1},\\ &S_{ij}^*=\frac{d_1 S_{ij}}{c\alpha}, \beta_i^*=\frac{\beta_i(i=2,3)}{d_1}, \chi=\frac{F-F_0}{F_1-F_0}, \xi=\frac{F_0}{F_1-F_0}.\end{aligned} \tag{17}$$

in equations (5)–(13). We can write after omitting asterisk

$$\frac{\partial^2}{\partial y^2}\left[\frac{\partial^2\psi}{\partial y^2}\left\{\left(\Omega\left(\frac{\partial^2\psi}{\partial y^2}\right)^2+1\right)^{\frac{n-1}{2}}\right\}\right]-M^2\frac{\partial^2\psi}{\partial y^2}+Gr\frac{\partial\theta}{\partial y}+Gc\frac{\partial\phi}{\partial y}+Gf\frac{\partial\chi}{\partial y}=0, \tag{18}$$

Table 1
Rate of heat transfer against different parameters.

Parameters								$-\theta'(\eta)$	
Rn	β_2	Gf	Gr	Pe	Nb	Ω	M	ND solve	bvp4c
0.1	0.1	0.5	0.5	2	1	0.1	0.5	0.180764	0.180678
1								0.022788	0.022667
1.5	0.2							0.192694	0.192599
	0.3							0.243157	0.243101
	0.1	0.7						0.115863	0.115698
		1						0.079072	0.078893
		0.5	0.7					0.256174	0.078893
			0.9					0.410292	0.410153
			0.5	2.5				0.157517	0.157449
				3				0.171638	0.171521
				2	1.5			0.177495	0.177347
					2			0.206790	0.206673
					1	0.2		0.107321	0.107201
						0.3		0.083210	0.083101
						0.1	0.8	0.110246	0.110119
							2	0.064198	0.064078

$$(1+\Pr Rn)\frac{\partial^2\theta}{\partial y^2}+Nb\Pr\frac{\partial\varphi}{\partial y}\frac{\partial\theta}{\partial y}+Nt\Pr\left(\frac{\partial\theta}{\partial y}\right)^2+BrM^2\left(\frac{\partial\psi}{\partial y}\right)^2+BrS_{xy}\frac{\partial^2\psi}{\partial y^2}=0, \tag{19}$$

$$Nt\frac{\partial^2\theta}{\partial y^2}+Nb\frac{\partial^2\phi}{\partial y^2}=0, \tag{20}$$

$$\frac{\partial^2\chi}{\partial y^2}-Pe\left(\frac{\partial\chi}{\partial y}\frac{\partial\phi}{\partial y}+\xi\frac{\partial^2\phi}{\partial y^2}+\chi\frac{\partial^2\phi}{\partial y^2}\right)=0 \tag{21}$$

The boundary conditions becomes

$$\frac{\partial\psi}{\partial y}\pm\beta_1\left\{\left(1+\Omega\left(\frac{\partial^2\psi}{\partial y^2}\right)^2\right)^{\frac{n-1}{2}}\right\}\frac{\partial^2\psi}{\partial y^2}=0 \text{ at } \ y=\pm\eta, \tag{22}$$

$$\left[E_1\frac{\partial^3}{\partial x^3}+E_2\frac{\partial^3}{\partial x\partial t^2}+E_3\frac{\partial^2}{\partial x\partial t}\right]\eta=\frac{\partial^3\psi}{\partial y^3}+\frac{\partial}{\partial y}\left\{\left(1+\Omega\left(\frac{\partial^2\psi}{\partial y^2}\right)^2\right)^{\frac{n-1}{2}}\right\}-M^2\frac{\partial\psi}{\partial y}+ \\ Gr\theta+Gc\phi+Gf\chi \text{at} y=\pm\eta, \tag{23}$$

$$\theta\pm\beta_2\frac{\partial\theta}{\partial y}=\left\{\begin{matrix}1\\0\end{matrix}\right\},\phi\pm\beta_3\frac{\partial\phi}{\partial y}=\left\{\begin{matrix}1\\0\end{matrix}\right\},\chi=\left\{\begin{matrix}1\\0\end{matrix}\right\}\text{at } \ y=\pm\eta. \tag{24}$$

Continuity equation (5) is automatically satisfied. In above expression we witnessed that the small Reynolds number and long wavelength assumptions [19] are invoked. Here δ, ε, Pr, Ec, Re , Sc, M, Nt, Br, Nb, Rn, Ω, Pe, Gr, (E_1, E_2, E_3), Gf, Gc ,are wave number, ratio of amplitude, Prandtl variable, Eckert variable, Reynolds number, Schmidt number, Hartman variable, thermophoresis parameter, Brinkman number, Brownian motion variable, Radiation parameter, Sisko fluid parameter, Bioconvection Peclet number, thermal Grashof number, wall parameteres, Bioconvection Rayleigh number, concentration Grashof variable. These are identified as [36,45]

$$\begin{gathered}\delta=\frac{d_1}{\lambda},\varepsilon=\frac{a}{d_1},\Pr=\frac{\nu}{\alpha},Ec=\frac{c^2}{c_f(T_1-T_0)},\mathrm{Re}=\frac{\rho c d_1}{\mu},Sc=\frac{\nu}{D_B},M=\sqrt{\frac{\sigma}{\mu}}B_0d_1,\\ Nt=\frac{D_T\tau(T_1-T_0)}{T_m\nu},Br=\Pr Ec,Nb=\frac{D_B\tau(C_1-C_0)}{\nu},Rn=\frac{16\bar{\sigma}T_0^3}{3\bar{k}\bar{k}},\Omega=\frac{\varsigma}{\alpha}\left(\frac{c}{d_1}\right)^{n-1},\\ Pe=\frac{bW_c}{D_m},Gr=\frac{g\beta_T(1-F_0)\rho_f(T_1-T_0)d_1^2}{\mu c},E_1=-\frac{d_1^3\tau}{\lambda\mu c},E_2=\frac{cm_1d_1^3}{\lambda^3\mu},E_3=\frac{d_1^3d}{\lambda^2\mu},\\ Gf=\frac{(\rho_m-\rho_f)g\gamma(F_1-F_0)d_1^2}{\mu c},Gc=\frac{g\beta_C(\rho_p-\rho_f)(C_1-C_0)d_1^2}{\mu c}.\end{gathered} \tag{25}$$

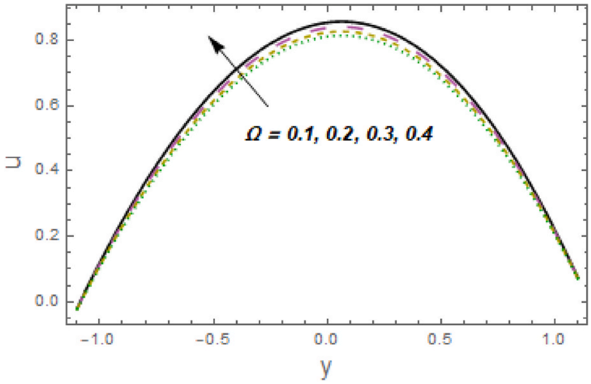

Fig. 2. u via Ω.

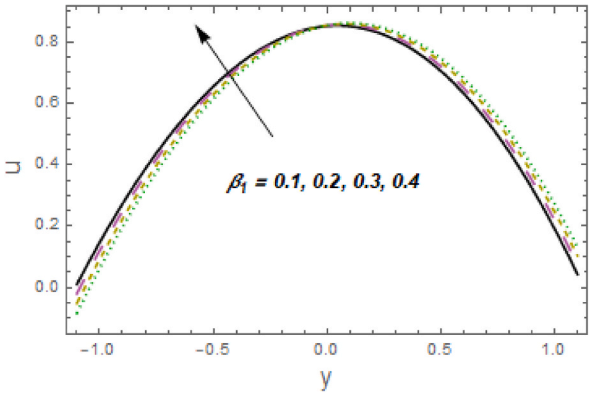

Fig. 3. u via β_1.

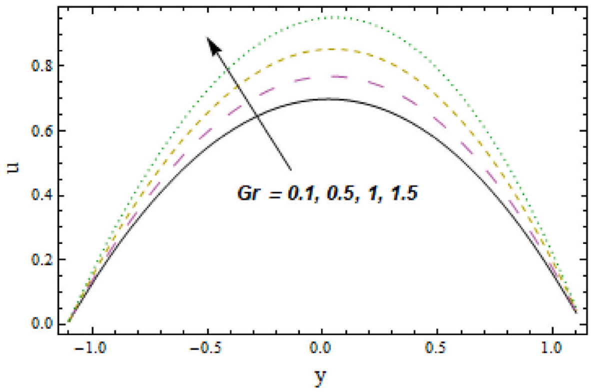

Fig. 4. u via Gr.

3. Numerical method

System of Eqs. (18)–(24) are solved numerically [5,9] by the command NDSolve by using the software Mathematica. In the meantime, many researchers used the bvp4c [51–53] solver available in the Matlab software to solve nonlinear ODEs. If the boundary error terms are below the tolerance error, 10^{-6}, the calculation simulation will converge. Table 1 for heat transfer rate is prepared to check the comparative analysis between the two utilized techniques, and the results show that both methods match in good agreement.

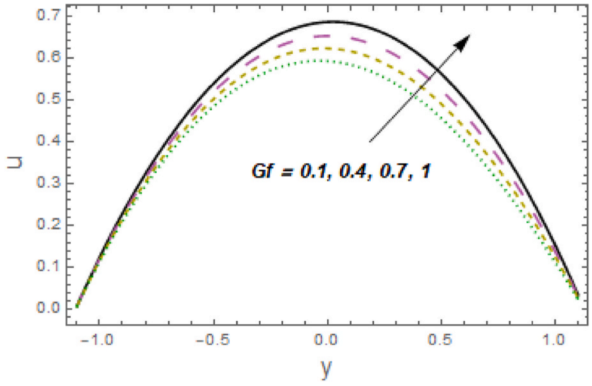

Fig. 5. u via Gf.

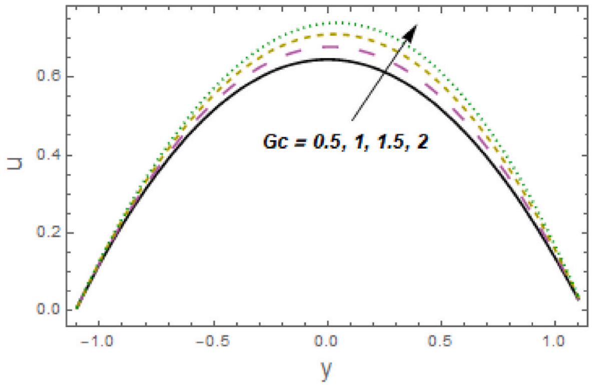

Fig. 6. u via Gc.

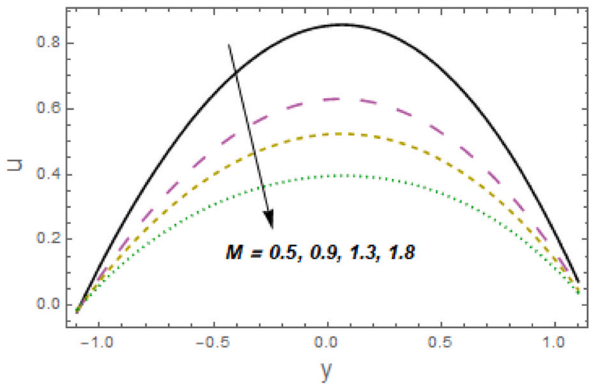

Fig. 7. u via M.

4. Results and discussion

This segment looked at the velocity profile, temperature, nanoparticle concentration, motile microorganisms density and rate of heat transfer.

4.1. Velocity

Figs. 2–8 are designed to see the features of pertinent variables like Sisko fluid variable Ω, velocity slip parameter β_1, Grashof parameter Gr, buoyancy ratio parameter Gc, Hartman number M, bioconvection Rayleigh variable Gf, wall parameters (E_1, E_2, E_3).

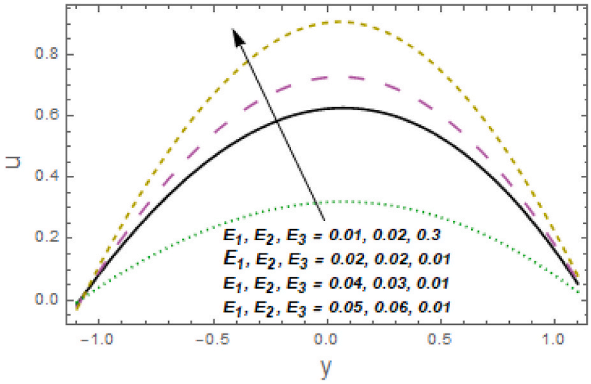

Fig. 8. u via E_1, E_2 and E_3.

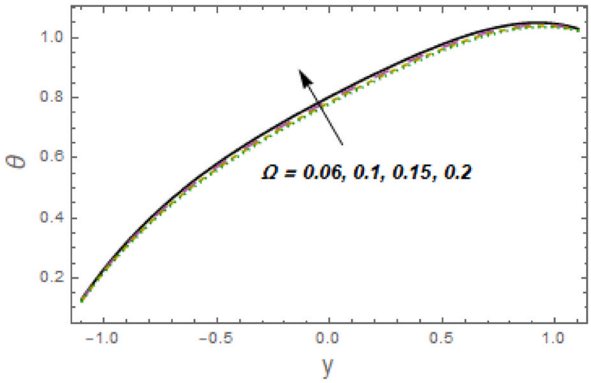

Fig. 9. θ via Ω.

Fig. 2 is sketched for sisko fluid variable. As you see in this Fig. velocity of the fluid enhances via sisko fluid variable Ω. Impact of velocity slip variable β_1 is exhibited by Fig. 3. It is detected that velocity enhances against β_1. This is due to the deference between the fluid velocity and surface velocity. Fig. 4 is aimed to see the consequence of Grashof number *Gr* on velocity. The outcomes of this graph revealed that as *Gr* rise, velocity of the liquid heightens. Fig. 5 demonstrates the consequence of bioconvection Rayleigh variable *Gf* on velocity profile by taking other constraints constant. The velocity profile reduces by enhancing *Gf*. Fig. 6 arranged to see the aspects of buoyancy ratio variable *Gc* on velocity profile. The graph demonstrates that the *Gc* increases the liquid's velocity. This is due to the buoyancy forces. Aspects of Hartman number *M* are portrayed via Fig. 7. From here we noticed that fluid velocity declensions. The Lorentz force was activated by the magnetic force, which causes reluctance and causes velocity decline. Effects of wall parameters E_1 , E_2 and E_3 are exhibited in Fig. 8. It is pointed out that velocity is an enhancing function of E_1 and E_2, and it drops for E_3..

4.2. Temperature

Consequences of different embedded variables on thermal field θ are examined through Figs. 9–17. To explore the effects of the Sisko fluid variable Ω, Fig. 9 is plotted. This figure demonstrates how the fluid's temperature increases as greater Ω. The effect of the thermal slip parameter β_2 is displayed in Fig. 10. It can be seen in this graph that the temperature of the fluid enhances via larger β_2. The impact of the Brinkman variable *Br* on temperature is depicted in Fig. 11. Temperature increases when the effects of viscous dissipation are amplified by a high Brinkman variable *Br*. Fig. 12 establishes the expressions of Grashof parameter *Gr* against temperature. An enhancement in temperature is observed from these results. A higher Grashof number enhances temperature transfer because it signifies that buoyancy-driven natural convection is significant, leading to increased fluid motion and improved heat transfer between hot and cold surfaces. The impacts of Hartman number *M* on the thermal field are revealed in exhibited in Fig. 13. It is evident from this figure that the temperature of the liquid declines. Fig. 14 is designed to show how the bioconvection Peclet number *Pe* affects temperature. It is discovered that as *Pe* raises, the fluid's temperature enhances. In Fig. 15, the thermal field's effect on the radiation parameter *Rn* is depicted. When the radiation parameter rises, the fluid's thermal field lessens. Fig. 16 depicts how the temperature is affected by the compliance variables E_1, E_2, and E_3. Results of this experiment reveal that the fluid's temperature rises via E_1 and E_2, but E_3 exhibits the reverse tendency. Fig. 17 depicts the temperature dependence of thermophoresis *Nt* and Brownian movement variables *Nb*. Both variables have significant increases in temperature. Brownian diffusion describes the impressions of random particle motion within a flow field. As Brownian diffusion increases, the fluid's mean kinetic energy rises, leading to a

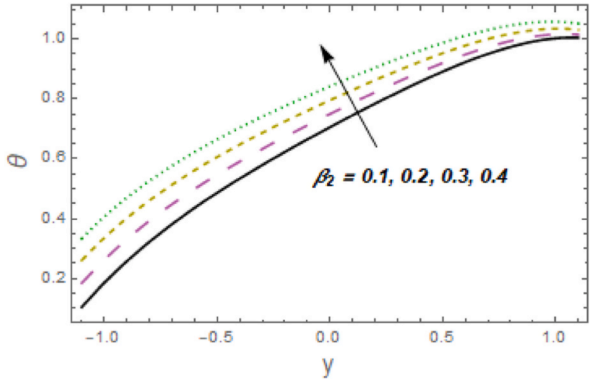

Fig. 10. θ via Ω.

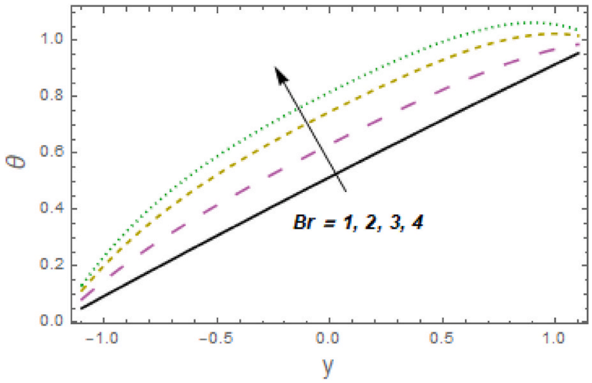

Fig. 11. θ via *Br*.

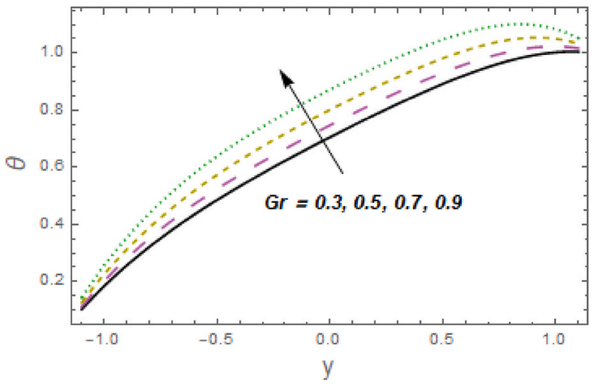

Fig. 12. θ via *Gr*.

corresponding increase in temperature gradients.

4.3. Concentration

Figs. 18–24 are designed to see the behavior of concentration field ϕ . Effect of bioconvection Peclet number *Pe* is demonstrated in Fig. 18 against concentration. It is noticed that concentration declines with larger bioconvection Peclet number *Pe*. It is due to the fact that the contribution of bioconvection to the transport of solute is decreasing compared to diffusion. Fig. 19 depicts the consequences of ξ on the concentration field. The detected consequences lay out that a boost in ξ diminishes the concentration. Features of buoyancy ratio parameter *Gc* against the concentration field are portrayed in Fig. 20. Results show that concentration of the liquid declines. The impacts of bioconvection depict the Rayleigh variable *Gf* (see Fig. 21). A detailed review of this pattern reveals that the nanoparticles

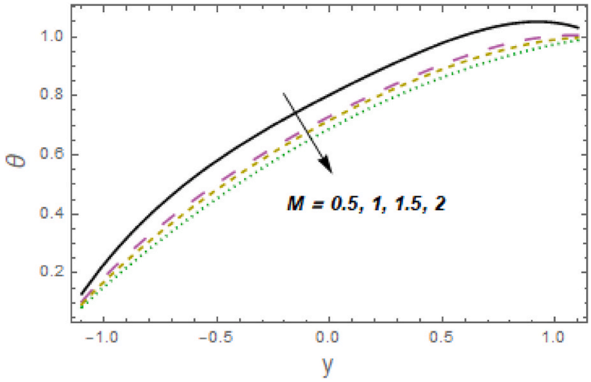

Fig. 13. θ via M.

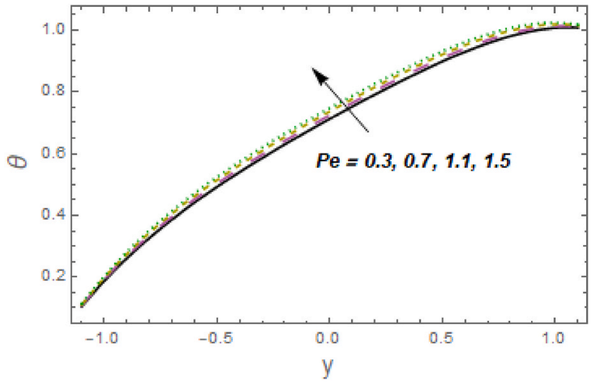

Fig. 14. θ via Pe.

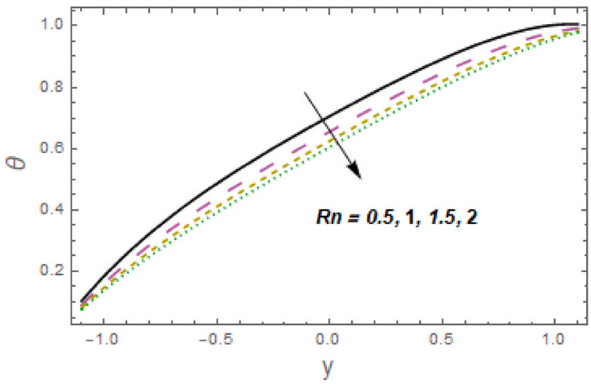

Fig. 15. θ via Rn.

concentration increases as Gf grows. Fig. 22 depicts the effect of thermophoresis Nt characteristics on nanoparticle concentration. This graph shows a downward trend. Physically, particles tend to migrate from regions of higher temperature to regions of lower temperature within a fluid. Impressions of wall parameters $(E)_{123}$ are presented in Fig. 23. It is found that concentration φ is an enhancing mapping of E_1 E_2, and it diminishes for E_3 in light of the dulling effect. The concentration field versus mass slip parameter β_3 is shown in Fig. 24. The concentration decreases as the mass slip parameter β_3 is increased.

4.4. Motile microorganism

Figs. 25–28 investigate the outcomes of pertinent parameters on profiles of motile microorganism χ. Aspects of bioconvection Peclet number Pe is exhibited in Fig. 25. As we discovered from this figure that motile microorganism profile χ decreases. Fig. 26

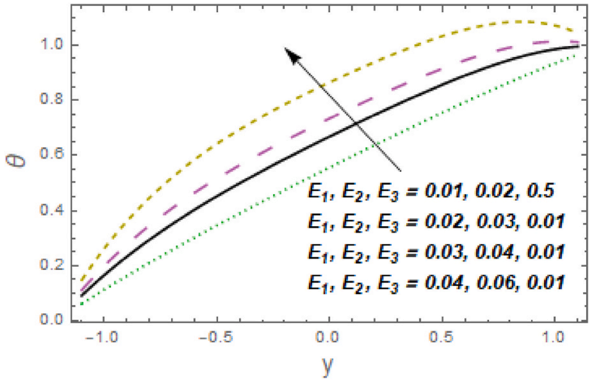

Fig. 16. θ via E_1, E_2 and E_3.

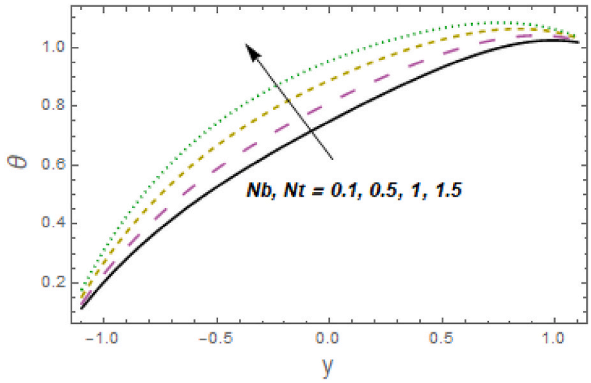

Fig. 17. θ via NbandNt.

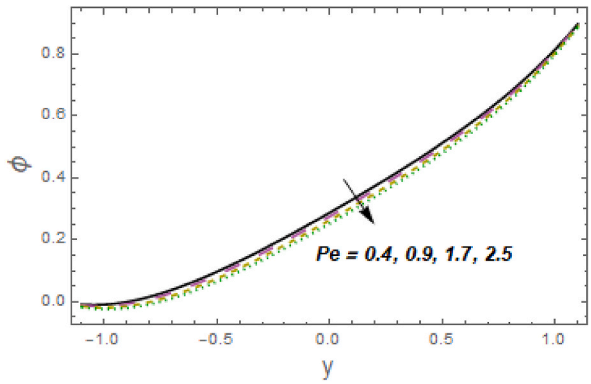

Fig. 18. ϕ via Pe.

represents to see the behavior of the Sisko fluid variable Ω on motile microorganism profile. Results show decaying behavior against this relevant parameter Ω. Results for ξ is illustrated in Fig. 27. With the enhancement of ξ profile of motile microorganism increases. Influence of bioconvection Rayleigh variable Gf on motile microorganism profiles is sketched through Fig. 28. It can be seen from this graph profile of motile microorganisms enhances.

4.5. Rate of heat transfer

Aspects of different parameters on heat transfer rate $-\theta'(\eta)$ are portrayed in Table 1. Rate of heat transfer rises by larger values of temperature slip variable β_2, Brownian movement variable Nb, bioconvection Peclet parameter Pe and Grashof number Gr. On the other side decreasing trend is noticed for radiation variable Rn, Hartman number M and Sisko fluid variable Ω..

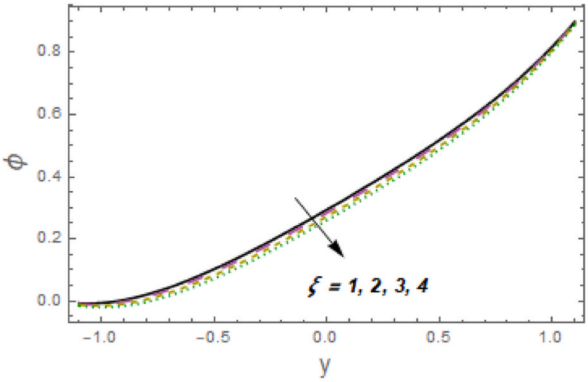

Fig. 19. ϕ via ξ.

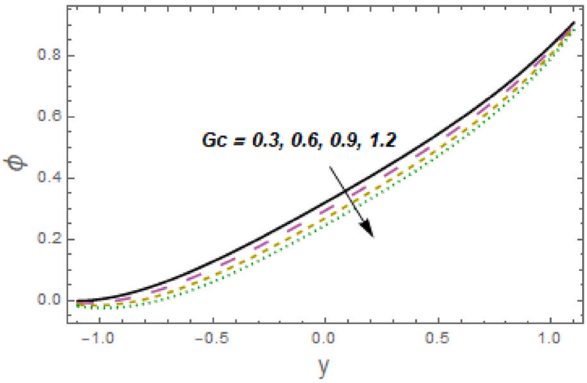

Fig. 20. ϕ via Gc.

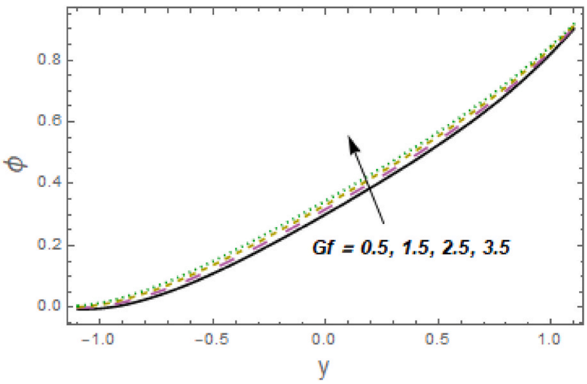

Fig. 21. ϕ via Gf.

5. Conclusions

In the present investigation we analyzed the impacts of bioconvection peristaltic flow of Sisko nanofluid in a symmetric elastic channel. Effects of thermal radiation and Joule heating considered. Numerical solutions are found for the governing nonlinear problem. It is found that velocity enhances Siko fluid parameter (Ω) and velocity slip parameter (β_1), while opposite trend is noticed for Hartman number (M). Temperature increases via larger Brinkman number (Br), bioconvection Peclet number (Pe) and Brownian motion parameter (Nb). Thermal radiation (Rn) shows similar behavior on heat transfer rate and temperature. Effects of buoyancy ratio parameter (Gc) and Rayleigh variable (Gf) on concentration are opposite. Motile microorganisms increase via bioconvection Rayleigh variable (Gf). Similar effects of Hartman number (M) and Sisko fluid parameter (Ω) are noted for heat transfer rate. Increase in bioconvection Peclet number (Pe) yields reduction in motile microorganisms. Heat transfer rate enhances via thermal slip parameter

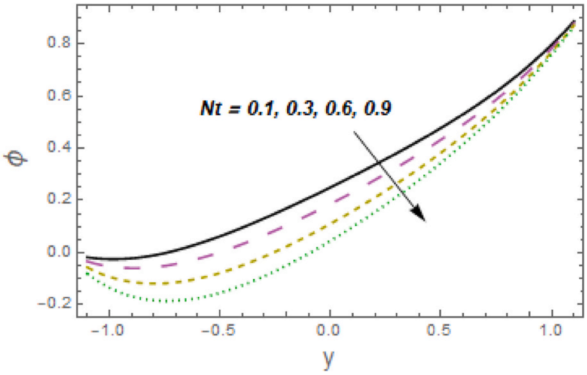

Fig. 22. ϕ via *Nt*.

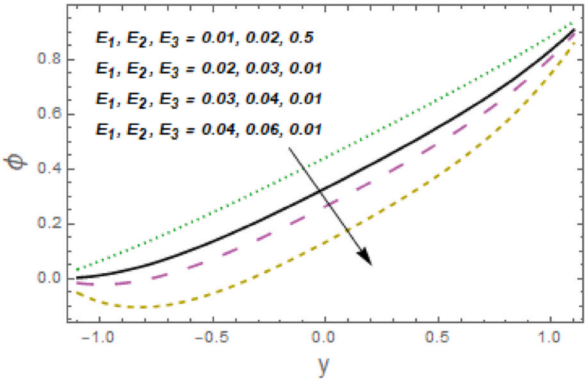

Fig. 23. ϕ via E_1, E_2 and E_3.

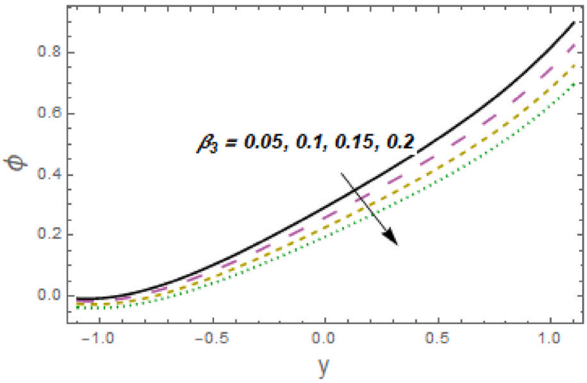

Fig. 24. ϕ via β_3.

(β_2) and bioconvection Peclet number (Pe)..

Data availability statement

Data will be made available on request.

CRediT authorship contribution statement

Zahid Nisar: Data curation, Methodology, Supervision, Writing – original draft. **Bilal Ahmed:** Data curation, Investigation, Methodology, Software. **Hassan Ali Ghazwani:** Data curation, Software, Visualization, Writing – review & editing. **Khursheed**

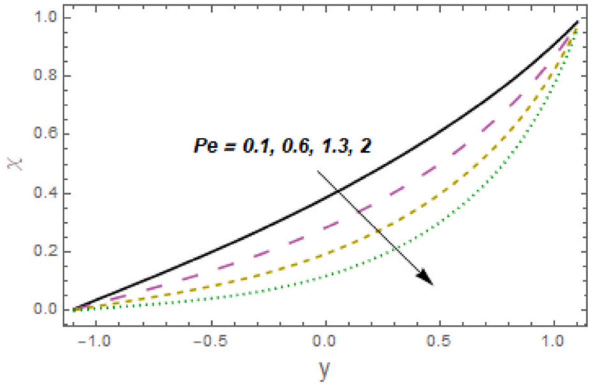

Fig. 25. χ via *Pe*.

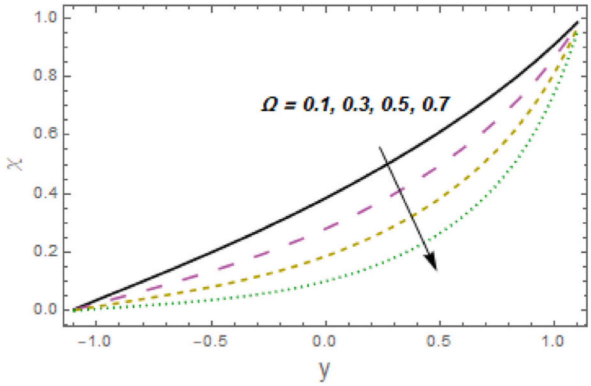

Fig. 26. χ via Ω.

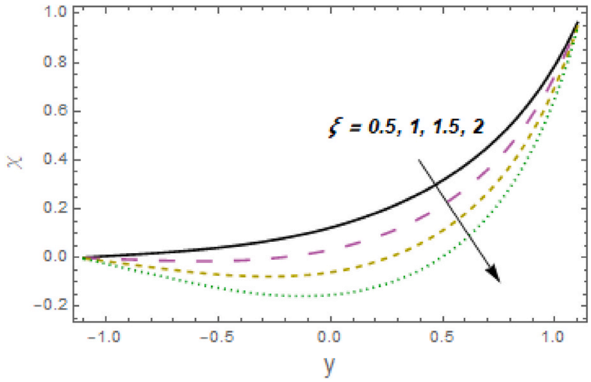

Fig. 27. χ via ξ.

Muhammad: Methodology, Software, Validation. **Mohamed Hussien:** Methodology, Software, Validation. **Arsalan Aziz:** Formal analysis, Software, Visualization, Writing – review & editing.

Declaration of competing interest

The authors declare that they have no known competing financial interests or personal relationships that could have appeared to influence the work reported in this paper.

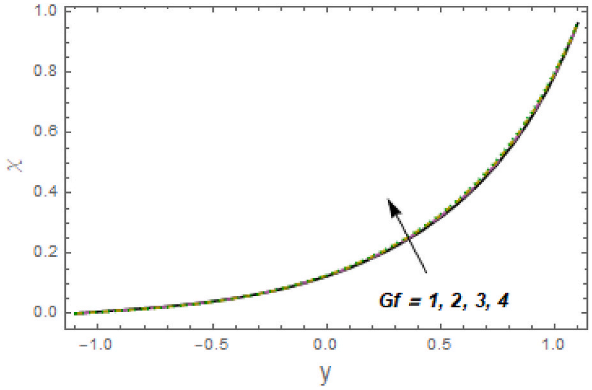

Fig. 28. χ via Gf.

Acknowledgements

The authors extend their appreciation to the Deputyship for Research & Innovation, Ministry of Education in Saudi Arabia for funding this research work through the project number ISP23-66.

References

[1] S.U.S. Choi, in: D.A. Siginer, H.P. Wang (Eds.), Enhancing Thermal Conductivity of Fluids with Nanoparticles, Developments and Applications of Non-newtonian Flows, vol. 231, 1995, pp. 99–105. ASME FED.
[2] J. Buongiorno, Convective transport in nanofluids, ASME J. Heat Transf. 128 (2006) 240–250.
[3] A. Ijam, R. Saidur, Nanofluid as a coolant for electronic devices (cooling of electronic devices), Appl. Therm. Eng. 32 (2012) 76–82.
[4] M. Mustafa, S. Hina, T. Hayat, B. Ahmad, Influence of induced magnetic field on the peristaltic flow of nanofluid, Meccanica 49 (2014) 521–534.
[5] T. Hayat, Z. Nisar, H. Yasmin, A. Alsaedi, Peristaltic transport of nanofluid in a compliant wall channel with convective conditions and thermal radiation, J. Mol. Liq. 220 (2016) 448–453.
[6] G. Sucharitha, P. Lakshminarayana, N. Sandeep, Joule heating and wall flexibility effects on the peristaltic flow of magnetohydrodynamic nanofluid, Int. J. Mech. Sci. 131 (2017) 52–62.
[7] F.M. Abbasi, M. Gul, S.A. Shehzad, Effectiveness of temperature-dependent properties of Au, Ag, Fe3O4, Cu nanoparticles in peristalsis of nanofluids, Int. Commun. Heat Mass Tran. 116 (2020), 104651.
[8] S. Akram, M. Athar, K. Saeed, Hybrid impact of thermal and concentration convection on peristaltic pumping of Prandtl nanofluids in non-uniform inclined channel and magnetic field, Case Stud. Therm. Eng. 25 (2021), 100965.
[9] T. Hayat, Z. Nisar, A. Alsaedi, B. Ahmad, Analysis of activation energy and entropy generation in mixed convective peristaltic transport of Sutterby nanofluid, J. Therm. Anal. Calorim. 143 (2021) 1867–1880.
[10] M. Khazayinejad, M. Hafezi, B. Dabir, Peristaltic transport of biological graphene-blood nanofluid considering inclined magnetic field and thermal radiation in a porous media, Powder Technol. 384 (2021) 452–465.
[11] A.S. Kotnurkar, V.T. Talawar, Influence of thermal jump and inclined magnetic field on peristaltic transport of Jeffrey fluid with silver nanoparticle in the eccentric annulus, Heliyon 8 (2022), e10543.
[12] Z. Nisar, T. Hayat, A. Alsaedi, S. Momani, Mathematical modelling for peristalticflow of fourth-grade nanoliquid with entropy generation, Z. Angew. Math. Mech. (2023), e202300034, https://doi.org/10.1002/zamm.202300034.
[13] N. Vinodhini, V.R. Prasad, Numerical study of magneto convective Buongiorno nanofluid flow in a rectangular enclosure under oblique magnetic field with heat generation/absorption and complex wall conditions, Heliyon 9 (2023), e17669.
[14] S.I. Abdelsalam, A.M. Alsharif, Y.A. Elmaboud, A.I. Abdellateef, Assorted kerosene-based nanofluid across a dual-zone vertical annulus with electroosmosis, Heliyon 9 (2023), e15916.
[15] Z. Nisar, T. Hayat, B. Ahmed, A. Alsaedi, Analysis of nonlinear radiative peristaltic transport of hyperbolic tangent nanomaterial with chemical reaction, Int. J. Mod. Phys. B (2023), 2450215.
[16] K. Muhammad, T.A. Assiri, S.I. Shah, I.E. Elseesy, Three-dimensional MHD flow of hybrid material between rotating disks with heat generation, Heliyon 9 (2023), e18018.
[17] M. Alghamdi, B. Fatima, Z. Hussain, Z. Nisar, H.A. Alghamdi, Peristaltic pumping of hybrid nanofluids through an inclined asymmetric channel: a biomedical application, Mater. Today Commun. 35 (2023), 105684.
[18] T.W. Latham, Fluid Motion in a Peristaltic Pump, MS Thesis, MIT, Cambridge, MA, 1966.
[19] A.H. Shapiro, M.Y. Jaffrin, S.L. Weinberg, Peristaltic pumping with long wavelength at low Reynolds number, J. Fluid Mech. 37 (1969) 799–825.
[20] S. Srinivas, M. Kothandapani, Peristaltic transport in an asymmetric channel with heat transfer-a note, Int. Commun. Heat Mass Tran. 35 (2008) 514–522.
[21] N. Ali, M. Sajid, T. Javed, Z. Abbas, Heat transfer analysis of peristaltic flow in a curved channel, Int. J. Heat Mass Tran. 53 (2010) 3319–3325.
[22] T. Hayat, S. Noreen, M.S. Alhothuali, S. Asghar, A. Alhomaidan, Peristaltic flow under the effects of an induced magnetic field and heat and mass transfer, Int. J. Heat Mass Tran. 55 (2012) 443–452.
[23] F.M. Abbasi, T. Hayat, A. Alsaedi, Numerical analysis for MHD peristaltic transport of Carreau-Yasuda fluid in a curved channel with Hall effects, J. Magn. Magn Mater. 382 (2015) 104–110.
[24] M.D. Sinnott, P.W. Cleary, S.M. Harrison, Peristaltic transport of a particulate suspension in the small intestine, Appl. Math. Model. 44 (2017) 143–159.
[25] M. Rashid, K. Ansar, S. Nadeem, Effects of induced magnetic field for peristaltic flow of Williamson fluid in a curved channel, Physica A 553 (2020), 123979.
[26] Y. Akbar, F.M. Abbasi, Impact of variable viscosity on peristaltic motion with entropy generation, Int. Commun. Heat Mass Tran. 118 (2020), 104826.
[27] P. Gangavathi, S. Jyothi, M.S. Reddy, P.Y. Reddy, Slip and hall effects on the peristaltic flow of a jeffrey fluid through a porous medium in an inclined channel, Mater. Today Proc. (2021), https://doi.org/10.1016/j.matpr.2021.05.696.
[28] Z. Nisar, T. Hayat, A. Alsaedi, B. Ahmad, Mathematical modeling for peristalsis of couple stress nanofluid, Math. Methods Appl. Sci. 45 (2023) 11683–11701.
[29] Z. Abbas, M.Y. Rafiq, J. Hasnain, T. Javed, Peristaltic transport of a Casson fluid in a non-uniform inclined tube with Rosseland approximation and wall properties, Arabian J. Sci. Eng. 46 (2021) 1997–2007.

[30] Z. Nisar, T. Hayat, K. Muhammad, B. Ahmed, A. Aziz, Significance of Joule heating for radiative peristaltic flow of couple stress magnetic nanofluid, J. Magn. Magn Mater. 581 (2023), 170951.
[31] H. Yasmin, Z. Nisar, Mathematical analysis of mixed convective peristaltic flow for chemically reactive Casson nanofluid, Mathematics 11 (2023) 2673.
[32] A.W. Sisko, The flow of lubricating greases, Ind. Eng. Chem. 50 (1958) 1789–1792.
[33] N.S. Akbar, Peristaltic Sisko nano fluid in an asymmetric channel, Appl. Nanosci. 4 (2014) 663–673.
[34] M.M. Bhatti, A. Zeeshan, R. Ellahi, Endoscope analysis on peristaltic blood flow of Sisko fluid with Titanium magneto-nanoparticles, Comput. Biol. Med. 78 (2016) 29–41.
[35] Z. Asghar, N. Ali, R. Ahmed, M. Waqas, W.A. Khan, A mathematical framework for peristaltic flow analysis of non-Newtonian Sisko fluid in an undulating porous curved channel with heat and mass transfer effects, Comput. Methods Progr. Biomed. 182 (2019), 105040.
[36] B. Ahmed, T. Hayat, A. Alsaedi, F.M. Abbasi, Joule heating in mixed convective peristalsis of Sisko nanomaterial, J. Therm. Anal. Calorim. 146 (2021) 1–10.
[37] S. Akram, M. Athar, K. Saeed, M.Y. Umair, Double-diffusive Convection with Peristaltic Wave in Sisko Fluids along with Inclined Magnetic Field and Channel, Waves Random Complex Media, 2021, pp. 1–23.
[38] A. Almaneea, Numerical study on thermal performance of Sisko fluid with hybrid nano-structures, Case Stud. Therm. Eng. 30 (2022), 101754.
[39] A. Tanveer, M.B. Ashraf, Mixed convective flow of Sisko nanofluids over a curved surface with entropy generation and Joule heating, Arabian J. Sci. Eng. (2022) 1–13.
[40] Y. Akbar, H. Alotaibi, J. Iqbal, K.S. Nisar, K.A.M. Alharbi, Thermodynamic analysis for bioconvection peristaltic transport of nanofluid with gyrotactic motile microorganisms and Arrhenius activation energy, Case Stud. Therm. Eng. 34 (2022), 102055.
[41] A.S. Kotnurkar, N. Kallolikar, E.N. Thabet, Double-diffusive bioconvection effects on multi-slip peristaltic flow of Jeffrey nanofluid in an asymmetric channel, Pramana 97 (2023) 108.
[42] S.A. Hussein, S.E. Ahmed, A.A.M. Arafa, Electrokinetic peristaltic bioconvectiveJeffrey nanofluid flow with activation energy for binary chemical reaction, radiation and variable fluid properties, Z. Angew. Math. Mech. 103 (2023), e202200284.
[43] J. Iqbal, F.M. Abbasi, M. Alkinidri, H. Alahmadi, Heat and mass transfer analysis for MHD bioconvection peristaltic motion of Powell-Eyring nanofluid with variable thermal characteristics, Case Stud. Therm. Eng. 43 (2023), 102692.
[44] J. Ahmed, F. Nazir, B.M. Fadhl, B.M. Makhdoum, Z. Mahmoud, A. Mohamed, I. Khan, Magneto-bioconvection flow of Casson nanofluid configured by a rotating disk in the presence of gyrotatic microorganisms and Joule heating, Heliyon 9 (2023), e18028.
[45] Z. Nisar, H. Yasmin, Analysis of motile gyrotactic micro-organisms for the bioconvection peristaltic flow of Carreau-Yasuda bionanomaterials, Coatings 13 (2023) 314.
[46] I. Ullah, M.T. Rahim, H. Khan, Application of Daftardar Jafari method to first grade MHD squeezing fluid flow in a porous medium with slip boundary condition, Abstr. Appl. Anal. 2014 (2014), 479136.
[47] I. Ullah, M.T. Rahim, H. Khan, M. Qayyum, Analysis of various semi-numerical schemes for magnetohydrodynamic (MHD) squeezing fluid flow in porous medium, Propuls. Power Res. 8 (2019) 69–78.
[48] I. Ullah, H. Khan, M.T. Rahim, Approximation of first grade MHD squeezing fluid flow with slip boundary condition using DTM and OHAM, Math. Probl Eng. 2013 (2013), 816262.
[49] I. Ullah, M.T. Rahim, H. Khan, M. Qayyum, Homotopy analysis solution for magnetohydrodynamic squeezing flow in porous medium, Adv. Math. Phys. 2016 (2016), 3541512.
[50] I. Ahmed, M. Alghamdi, M. Amjad, F. Aziz, T. Akbar, T. Muhammad, Numerical investigation of MHD flow of hyperbolic tangent nanofluid over a non-linear stretching sheet, Heliyon 9 (2023), e17658.
[51] K. Muhammad, T. Hayat, A. Alsaedi, Numerical study for melting heat in dissipative flow of hybrid nanofluid over a variable thicked surface, Int. Commun. Heat Mass Tran. 121 (2021), 104805.
[52] A. Ayub, Z. Sabir, G.C. Altamirano, R. Sadat, M.R. Ali, Characteristics of melting heat transport of blood with time-dependent cross-nanofluid model using Keller-Box and BVP4C method, Eng. Comput. 38 (2022) 3705–3719.
[53] D. Dey, B. Chutia, Two-phase fluid motion through porous medium with volume fraction: an application of MATLAB bvp4c solver technique, Heat Transf 51 (2022) 1778–1789.